Micro-X-Ray Fluorescence, Micro-X-Ray Absorption Spectroscopy, and Micro-X-Ray Diffraction Investigation of Lead Speciation after the Addition of Different Phosphorus Amendments to a Smelter-Contaminated Soil

Lucas R. Baker, Gary M. Pierzynski, Ganga M. Hettiarachchi, Kirk G. Scheckel and Matthew Newville

µXRF, µXAS and µXRD Investigation of Pb Speciation after the Addition of

Different P Amendments to a Smelter-Contaminated Soil

Lucas R. Baker[†], Gary M. Pierzynski[‡], Ganga M. Hettiarachchi[‡], Kirk G. Scheckel[§], and*

Matthew Newville[††].

[†]Brookside Laboratories, Inc. 308 S. Main Street, New Knoxville, OH, 45871;

[‡]Department of Agronomy, Throckmorton Plant Sciences Center, Kansas State

University, Manhattan, Kansas 66506-5501; [§]United States Environmental Protection

Agency, National Risk Management Research Laboratory, 5995 Center Hill Ave.,

Cincinnati, OH 45224; [††]Consortium for Advanced Radiation Sources, The University of

Chicago, 5640 S Ellis Ave., Chicago, IL 60637.

Corresponding author phone: (785)532-7200; fax: (785)532-6094; email: gmp@ksu.edu

Abstract

The stabilization of Pb upon additions of P to contaminated soils and mine spoil materials has been well documented. It is clear from the literature that different P sources result in different efficacies of Pb stabilization in the same contaminated material. We hypothesized that the differences in efficacy of Pb stabilization in contaminated soils upon fluid or granular P amendment addition is due to different P reaction processes in and around fertilizer granules and fluid droplets. We used a combination of several synchrotron-based techniques, namely, spatially resolved micro-x-ray fluorescence (μ-XRF), micro-x-ray absorption near edge structure spectroscopy (μ-XANES), and micro-x-ray diffraction (μ-XRD) to speciate Pb at two incubation times in a smelter contaminated soil upon addition of several fluid and granular P amendments. The results indicated that the Pb phosphate mineral plumbogummite was an intermediate phase of pyromorphite formation. Additionally, all fluid and granular P sources were able to induce Pb phosphate formation, but fluid phosphoric acid (PA) was the most effective with time and distance from the treatment. Granular phosphate rock (PR) and triple super phosphate (TSP) amendments reacted to generate Pb phosphate minerals, with TSP being more effective at greater distances from the point of application. As a result, PA and TSP were the most effective P amendments at inducing Pb phosphate formation, but caution needs to be exercised when adding large additions of soluble P to the environment.

Introduction

Lead (Pb) is a natural constituent of all soils (Adriano, 2001).   Soil Pb concentrations have increased in past years through such processes as mining, sewage sludge application, fossil fuel combustion, and many chemical and other manufacturing

industries (Adriano, 2001; Basta et al., 2005). A wide variety of health effects of Pb exposure in children and adults have been recognized (ATSDR, 2005), and according to recent reports, no safe blood Pb threshold for children has been identified to date (Brown and Margolis, 2012). Lead contaminated soil is a primary source of Pb exposure to young children. It is well known that different soils with same total Pb concentrations could have very different bioavailable Pb concentrations (Scheckel et al, 2009). The bioavailability of Pb in soils and mine wastes primarily depends on its chemical speciation (Scheckel and Ryan, 2004). In contaminated soils and mine wastes, large fractions of Pb can exist in potentially bioavailable fractions. Therefore, considerable effort has been focused on developing cost-effective remediation technologies to reduce metal bioavailability and mobility in natural environments (Ryan et al., 2004).

Previously, remediation efforts have principally consisted of removal of the contaminated material with subsequent back-filling with clean soil. However, this process is costly, time consuming, and requires a source of clean soil. Current research involves the potential to change the bioavailability of Pb *in situ* by altering its chemical speciation (Mench et al., 1994, Porter et al., 2004). Much of this research has been focused on the addition of P amendments to Pb contaminated soils to form Pb phosphates, particularly pyromorphite, which is one of the most stable Pb minerals under a wide range of environmental conditions (Nriagu, 1974). As a result, P amendments could be used to reduce the bioavailability/bioaccessibility of Pb in contaminated soils and mine wastes.

Immobilizing Pb as pyromorphite in soils has been extensively studied in the literature (Cao et al., 2003; Chappell and Scheckel, 2007; Chen et al., 2006; Cotter-

Howells and Caporn, 1996; Hashimoto et al., 2009; Hettiarachchi and Pierzynski., 2004; Hettiarachchi et al., 2000; Hettiarachchi et al., 2001; Lin et al., 2005; Ma et al., 1993, 1995; McGowen et al., 2001; Ruby et al., 1994; Scheckel and Ryan, 2002; Scheckel and Ryan, 2004; Yang et al., 2001; Yoon et al., 2007). The possibilities of inadequate immobilization, or dissolution of pyromorphite after P treatment, have also been investigated (Butkus and Johnson, 2011; Debela et al., 2010).

Research has continued to explore the effect of different P sources on metal phosphate formation. These sources include phosphate rock (PR), diammonium phosphate (DAP), triple superphosphate (TSP), and phosphoric acid (PA) (Cao et al., 2003; Chappell and Scheckel, 2007; Hettiarachchi et al., 2000; Hettiarachchi et al., 2001; McGowen et al., 2001; Yang et al., 2001). All P sources have resulted in the reduction of Pb bioavailability to a variety of organisms. This decline is hypothesized to be the result of metal phosphate formation. However, treatment effects could vary across soils due to the chemical heterogeneity of soil environments. Additionally, it is not well understood how the metal phosphate species formed might be influenced by P source or by distance in the soil from P-containing materials, which has implications for the amount of P that needs to be added and the degree of mixing that is required. For example, fluid P delivery systems should be more effective at producing metal phosphates due to the greater solubility of P for reaction and a larger reaction zone due to greater diffusion. However, research in this area is lacking and is needed to better understand the influence of P sources in the Pb sequestration process.

Understanding the rate and effectiveness of P treatments on the sequestration of Pb as Pb phosphates, more specifically pyromorphites, methodologies that is capable of examining

true speciation of soil Pb *in situ* must be employed. So one goal of Pb stabilization research is to measure the amount of soil Pb that is converted to less soluble phosphate phases, but this is problematic in heterogeneous, non-equilibrated systems (Scheckel and Ryan, 2004). More recently, speciation of metals in complex environments has been achieved by using spatially-resolved synchrotron-based techniques, such as X-ray absorption spectroscopy (XAS), coupled with statistical analysis via linear combination fitting (LCF) or principal component analysis (PCA) (Hashimoto et al., 2009; Isaure et al., 2002, Roberts et al., 2002, Scheckel and Ryan, 2004). This experimental approach combines the *in situ* capabilities of synchrotron-based techniques with thorough statistical analysis that allows one to compare unknown samples to well-characterized reference compounds (Scheckel and Ryan, 2004). Concerns with this procedure do exist because of the limited number of reference mineral compounds, but it has been suggested that the combined use of different synchrotron-based techniques could enhance mineral species identification (Manceau et al., 2002a). Therefore, a combination of μ-X-ray fluorescence (μ-XRF), μ-XAS, and μ-X-ray diffraction (μ-XRD) would allow one to locate trace-metal enriched areas (μ-XRF), understand the approximate chemical environment (μ-XAS), and identify the mineral form (μ-XRD). This approach was employed to accomplish the following objectives: 1) investigate how different P sources influence the Pb phosphate species formed, 2) estimate the relative abundance of the Pb phosphate minerals formed at a given distance from the P amendment, and 3) observe how Pb speciation changes with reaction time.

Materials and Methods

Materials. The material used in this study was collected from an abandoned Pb/Zn smelter near Dearing, KS.   The material was collected from the upper 20 cm, sieved through a stainless steel 2-mm screen, air dried, and stored in plastic containers at room temperature. This material is a smelter slag/soil mixture that has been previously studied to evaluate the effect of different P treatments on reduction of bioavailability (determined by physiologically based extraction test, PBET), and solubility of Pb (determined by toxicity characteristics leaching procedure, TCLP) (Hettiarachchi et al., 2000; Hettiarachchi et al., 2001).

Soil pH was measured in a 1:1 deionized water:soil mixture with a Ross Combination pH electrode (Thermo Orion, Beverly, MA). Total organic C was measured by dry combustion on a LECO CN-2000 Elemental Analyzer (LECO Corporation, St. Joseph, MI). Samples were treated with phosphoric acid prior to analysis to remove the carbonates.   Total P for contaminated soil and P amendments were determined by salicylic-sulfuric acid digestion (Bremner and Mulvaney, 1982) and extractable P by Mehlich-3 (Mehlich, 1984). Filtered digests/extracts were then analyzed colorimetrically for P content. Cation exchange capacity (CEC) was determined by ion displacement (Jaynes and Bigham, 1986).   Nitric-acid extractable metal concentrations were determined by digesting 2 g of material ($\leq$ 2-mm) with 20 mL of 4 M HNO_3 (trace metal grade) acid at 80 to 85°C for 4 h (Sposito et al., 1982).   Filtered digests were then analyzed for Cd, Pb, and Zn by inductively coupled plasma-optical emission spectrometry (ICP-OES). Total "free" iron oxide content was estimated using the Na-citrate bicarbonate-dithionite method (Na-CBD) (Jackson et al., 1986).   Extracts were analyzed for Fe using ICP-OES. Soil was analyzed for sand, silt and clay content by the

pipette method as described by Gee and Bauder (1986). See Table 1 for details. For bulk

X-ray analyses, fractionation of sand, silt, and clay was done according to Jackson

(1975). The bulk X-ray analyses were conducted with a Phillips X-ray diffractormeter

(Phillips Electronic Instruments, Mahwah, NJ) with a theta compensating slit and curved

crystal graphite monochromator. Measurements were taken using Cu Kα radiation at a

wavelength of 1.54 Å and were made using a continuous scanning technique at a speed of

2° 2θ per minute. The potential was 35 kV, and the amperage 20mA.

Sample Preparation for X-ray Techniques. The treatments in this study included

several P sources and a control that were reacted over two different time periods (4 and

52 weeks). The P sources included fluid phosphoric acid (PA) and ammonium

polyphosphate (APP) and the granular sources phosphate rock (PR), monammonium

phosphate (MAP), and triple super phosphate (TSP). In addition, a contaminated non-P

amended control was prepared for comparison. MAP, APP, and TSP were commercially

available fertilizer grade P sources and contained 221, 133, and 199 g P kg^{-1},

respectively. MAP and APP contain N in the ammonium form and each delivered 115

and 102 g N kg^{-1}, respectively. The PR (powder form) was from Occidental Corp.

(White Springs, FL) and had 144 g P kg^{-1}, while PA was technical grade phosphoric acid

containing 314 g P kg^{-1}. For each treatment combination, one hundred-g (dry weight

basis) of contaminated waste material (25% gravimetric water content) was placed in a

plastic container. The P sources were added in a line across (40 mm deep) the center of

the container so that 20 mg of P were provided by each source. The amount of P added

reflected an average for a typical granule of the dry fertilizer materials. The P additions

were clearly marked with plastic toothpicks and covered by additional contaminated

material. The containers were packed to a bulk density of 1.35 g cm^{-3}. The plastic containers were covered with Parafilm, which would not make containers fully air-tight, and allowed to incubate in the moist condition for 4 or 52 weeks. No additional water was added during the incubation. Once incubation time was 24 hours from being complete, the covers were removed from the plastic containers, and they were placed in the greenhouse to air dry. The air-dried samples were then impregnated with Buehler EpoThin® two part (epoxy/hardener) resin (Beuhler LTD., Lake Bluff, IL, USA) and allowed to cure overnight. The hardened resin was then cut using a petrographic trim saw to expose the P treatments and surrounding waste material. Once exposed, the surface was polished to remove saw markings, cleaned with deionized water, dried, and cemented to polystyrene plastic (0.5-mm thick) using Hillquist Thin Section Epoxy A-B (Hillquist Inc., Denver, CO, USA). Polystyrene plastic was chosen instead of glass in an attempt to eliminate as much background noise in µ-XRD measurements. Once the cement was dry, thin sections were polished to a thickness of approximately 25-µm.

Synchrotron-based µ-XRF, -XAS, and -XRD Data Collection/Analyses. Micro-XRF maps, µ-XAS, and µ-XRD were collected at beamline 13-BM (GeoSoilEnviro Consortium of Advanced Radiation Sources) at the Advanced Photon Source at Argonne National Laboratory, Argonne, IL. All data were collected at ambient temperature in fluorescence mode with a Ge solid-state 13-element detector (Canberra Inc., Meriden, CT, USA) and µ-XRD spectra were collected with a MAR 345 Image Plate detector (MarUSA Inc., Evanston, IL, USA).

The samples were mounted on an x-y-θ stepping-motor stage. Fluorescence data for Pb were collected at ambient temperature for a given area (map sizes typically range

from 3000- by 6000-μm) for all fluid and granular P treatments with a step size of 50-μm. Using the XRF maps, further investigation of four to six points of interest (POIs) (high relative concentrations) for Pb were determined moving outward from the point of P application. Figure 1 illustrates how POIs were selected. For granular sources, the centers of the point of application for different treatments were defined by the granule. Whereas in fluid treatments, the center of the point of application was estimated by distance from a plastic marker (toothpick) installed at the time of P application.

For each sample, three replicates of μ-XAS spectra for each defined Pb POI were collected across the range of -200 to 600 eV above the L_{III}-edge of Pb (~13035 eV) in fluorescence mode and spot size was about 25-30 μm. The μ-XAS spectra were also collected for several known standard Pb compounds in transmission mode (Figure 2A). Standard Pb compounds include galena [PbS], anglesite [$PbSO_4$], cerussite [$PbCO_3$], hydrocerussite [$Pb_3(CO_3)_2(OH)_2$], leadhillite [$Pb_4(SO_4)(CO_3)_2(OH)_2$], magnetoplumbite [$PbFe_6Mn_6O_{19}$], plumboferrite [$Pb_2Mn_{0.2}Mg_{0.1}Fe_{10.6}O_{18.4}$], plumbojarosite [$PbFe_6(SO_4)_4(OH)_{12}$], plumbogummite [$PbAl_3(PO_4)_2(OH)_5 \cdot H_2O$], vaquelinite [$Pb_2Cu(CrO_4)(PO_4)(OH)$], hinsdalite [$PbAl_3(PO_4)(SO_4)(OH)_6$], and pyromorphite [$Pb_5(PO_4)_3Cl$]. In addition, the μ-XAS spectra were also collected for Pb sorbed to ferrihydrite at pH of 6.

The collected Pb μ-XAS spectra for P treatments and reference compounds were processed using the IFEFFIT software package (Ravel and Newville, 2005). Due to the poor quality of the extended x-ray absorption fine structure region only μ-XANES spectra could be used for Pb data analysis. A minimal smoothing was done using IFEFFIT software by applying a simple three-point smoothing algorithm while

comparing carefully with the unsmoothed spectra. Processed experimental spectra were analyzed in a two-step process using Labview software for principal components analysis (PCA) and the IFEFFIT software package for linear combination fitting (LCF) (Ravel and Newville, 2005). Principal components analysis was used prior to LCF only to test the consistency of the fitting procedure and, therefore, results from PCA will not be presented. The number of significant components determined by PCA was four based either on the minimum indicator (IND) value of each component or on the weight of each component, which is directly related to how much of the signal it represents. Based on PCA analysis, maximum number of components was limited to four during the LCF. The region of 12985 to 13135 eV for Pb was isolated for Pb LCF. The linear combination procedure was performed to reconstruct the contaminated soil-P amendment spectra using all of the combinations of the all reference spectra.

For the LCF procedure, the combination with the lowest reduced χ^2 was chosen as the most likely set of components. The accuracy of LCF depends on the data quality and how well the reference spectra fit the experimental samples (Roberts et al., 2002). A reduced χ^2 value near 1 indicates a reliable fit. Because there are a limited number of reference spectra and problems obtaining ideal standards to use in the fits, the best-fit compositions may not give the true composition, but the results can be used to describe and compare the differences between treatments. To help remedy this problem, synchrotron-based μ-XRD can be teamed with μ-XAS to enhance mineral species identification (Manceau et al., 2002a; 2002b). X-ray diffraction is a more definitive technique than XAS, but minerals have to be crystalline in order to utilize XRD. Therefore, a μ-XRD (~17,500 eV) pattern was taken at each Pb POI to assist in species

identification. For μ-XRD spectra, the data were processed using the Fit2D software package for integrating 2D Debye-Scherer rings to one-dimensional 2θ scans (Hammersley et al., 1996). The compound cerium dioxide (CeO_2) was used as the calibrant. Cerium was chosen because it is a relatively heavy element, so it will diffract higher energy X-rays very strongly. D-spacings were calculated using Fit2D software and matched to the d-spacings of known mineral species using the powder diffraction file search manual (JCPDS-International Centre for Diffraction Data, 1987).

To elucidate information on the movement and distribution of P upon the addition of P amendments, μ-XRF maps were collected at beamline 2-ID-D at the Advanced Photon Source, Argonne, IL. Thin sections, previously used at 13-BM, were peeled from the plastic slides and mounted onto a sample holder, which provided a sample thickness of approximately 25-μm. The sample holder was then placed on an x-y-θ stepping-motor stage. Fluorescence data for the P K-edge (2145.5 eV) were collected at ambient temperature for a 300- by 2000-μm area for all fluid and granular P treatments. A beam size of 500- by 500-nm with a step size of 5-μm was used and data were collected with a silicon drift detector. In addition, XRF spectra for two thin-film NIST multi-element standard reference materials (SRM 1832 and SRM 1833 for X-ray fluorescence spectrometry) were collected for conversion of XRF signals to relative elemental concentrations, which allows for the quantification of elements. MAPS software version 1.6.0.4 was used to quantify the distribution of P for each XRF map. Data was used to produce a plot of concentrations as a function of distance from the P amendment.

The effects of P amendments on Zn in this mine waste material and from this same incubation study has been reported separately (Baker et al., 2012). However, no

relationship exists between the POI's used here and those used for the Zn work. Areas enriched in Zn were not generally also enriched in Pb.

Results and Discussion

Bulk Mineralogical Analyses. Bulk XRD techniques can only detect crystalline materials present in concentrations $\geq$ 10 to 20 g kg^{-1} (Ma et al., 1994), and direct identification of solid forms of many elements was not always possible by XRD. The mineralogy of the silt- (0.05 mm to 0.002) and clay-sized (< 0.002 mm) fractions indicated the presence of quartz, willemite, and galena, but peak intensities for these minerals were weak, suggesting that the minerals were present at concentrations near the detection limit and/or poorly crystalline. The clay-sized fraction was enriched in Fe, implying the presences of Fe oxyhydroxide solid phases, which could influence the movement of P and the formation of Pb phosphates since such solids have a high affinity for phosphates (Table 1, Pierzynski and Sims, 2005). Unfortunately, comparable data was not collected for Al. There was no evidence for the existence of Pb phosphate minerals in either mineral fraction analyzed.

Synchrotron-based Pb speciation in non-amended soil. Bulk-XANES analysis of non-amended soil collected in the transmission mode indicated that the major Pb species were galena, cerussite and plumboferrite(Figure 2B, Table 4). Linear combination fitting showed relative abundances of 70% for galena, 20% for cerussite, and 10% for plumboferrite. According to μ-XANES the major Pb species present in non-amended soils include cerussite, galena, and sorbed Pb with smaller amounts of anglesite, magnetoplumbite, and plumboferrite (Table 2). Although μ-focused XANES alone

would not be sufficient to assess the "average" molecular environment surrounding the element of interest it allows identification of minor species because we probe limited soil volume at a given time and that might be the reasoning for observing more Pb species with μ-XANES. Because there were a limited energy range used for LCF procedure and a limited number of standard spectra, there was some uncertainty associated with the LCF procedure, μ-XRD analysis was used to further aid in species identification. Micro-XRD analysis of these samples confirmed the presence of cerussite (d-spacings of 3.59, 3.50, 2.49, 1.86, and 1.93) and galena (d-spacings of 2.97, 3.43, 2.10, and 1.79) for the control samples. No other Pb minerals were identified by μ-XRD in the control samples. Other studies, using either bulk or molecular techniques, have established that galena, anglesite, cerussite, pyromorphite, and sorbed Pb species are the dominant forms of Pb present in non-amended contaminated soils/mine tailings (Cao et al., 2002; Ostergren et al., 1999; Scheckel and Ryan, 2004; Hettiarachchi et al., 2001), which generally agrees with our data.

Synchrotron-based speciation changes of Pb upon P amendment addition. The LCF analysis of the Pb μ-XANES spectra for different P amendments indicated the presence of Pb phosphate minerals for all treatments in the contaminated soil (Table 2, Figure 2B). This implied that all P amendments were successful at converting Pb from more soluble species to the less soluble Pb phosphate minerals, namely plumbogummite and pyromorphite.   However, results vary by P amendment, incubation time, and distance from the point of P application.

For PR incubated for 4 weeks, plumbogummite (55%) was the major Pb species adjacent to the granule. However, Pb phosphate minerals became an insignificant part of

the fit as the distance from the PR granule increased, which was anticipated due to the low solubility of PR (Lindsay, 1979). After 52 weeks, the same trend still existed. There were significant amounts of Pb phosphates present adjacent to the granule, 26% plumbogummite and 19% pyromorphite, but as distance increased from 900 to 1200 μm the amount of plumbogummite decreased from 50% to 5%, respectively, which can again be attributed to the low solubility of PR.

To better illustrate the differences in P solubility, Figure 3 compares the average concentration of P with distance from the edge of a PR or TSP granule, and to PA droplet, relative to background soil P concentrations at 52 weeks. Phosphorus concentrations in the PR treatment reached background levels at approximately 1250 μm, which was the point where plumbogummite was estimated to be 4.9% of the Pb species present. In contrast, P concentrations for the fluid PA amendment were evenly dispersed and at appreciably higher concentrations than background levels up to 2000 μm. Distribution of P in granular MAP (data not shown) and TSP (Figure 3) were intermediate to PR and PA, while P concentration distribution in APP, another fluid P source, (data not shown) was similar to PA. These results support other studies that indicated reduced lability of granular P compared to liquid fertilizer formulations (Hettiarachchi et al., 2006; Lombi et al., 2005). This may influence the effectiveness of the P amendment at immobilizing Pb. In particular, greater available P concentrations created by both fluid and highly soluble granular P sources could enhance the probability of Pb phosphate formation. However, more soluble P sources could increase eutrophication risk if P amended soil or mine waste were moved off site into surface waters.

Linear combination fitting for the PA amendment incubated for 4 weeks showed a relatively even distribution of Pb phosphates with distance from the point of P application (Table 2). However, the identity of the P solid phases did vary. At the 52 week sampling, pyromorphite (38.5%) became the dominant Pb mineral adjacent to the droplet, while the amount of plumbogummite increased at 1500 and 3300 μm when compared to similar distances at the 4 week period. Additionally, it appeared as if the P gradient was nonexistent at 52 weeks in the PA treatment, which was supported by the μ-XRF generated radial P distribution plot (Figure 3). As a result, the same amount of P applied through fluid PA versus that applied in granular PR influenced the Pb chemistry of a much larger area. However, there is concern that PA will lower soil pH (Cao et al., 2003), which could subsequently alter the bioavailability of Pb and other potentially toxic metals (Yoon et al., 2007).

Fluid APP could be used to supply P for reaction with less acidity, but it has not been studied. After a 4 week incubation period, Pb phosphate minerals dominated the Pb speciation at 300 and 2400 μm from the point of APP application (Table 2). Additionally, this was the only amendment, either granular or fluid, besides TSP that induced pyromorphite formation within weeks of application. At 3600 μm, the amount of Pb phosphates was significantly reduced as compared to 300 and 2400 μm, which suggested that P had not yet diffused to this point or P availability was limited by another variable. At 52 weeks, pyromorphite was the principal Pb mineral adjacent to the droplet, while at 1700 and 4200 μm the amount of Pb phosphates decreased. In contrast, the radial distribution plot for APP at 52 weeks showed an even distribution pattern similar to PA (Figure 3), suggesting that Pb phosphate formation was limited by other

factors such as P sorption to Fe oxides (Sims and Pierzynski, 2005), lack of Pb for reaction, or competition of other metals for P (Lindsay, 1979; Nriagu, 1984).

Triple super phosphate, which is mostly monocalcium phosphate $[Ca(H_2PO_4)_2*H_2O]$, was the only granular P source to induce pyromorphite formation at the 4 week incubation period (Table 2). This could be attributed to the small amount of acidity produced during granule dissolution that could potentially release Pb for reaction. In addition, the amount of Pb phosphate minerals produced by TSP during this time period was rather homogenous over distance, similar to the fluid P sources. At 52 weeks, the amount of pyromorphite present increased with a subsequent decrease in plumbogummite when compared to the 4 week incubation. However, the amount of Pb phosphate minerals formed over the entire area did not increase dramatically with time, which suggested a rather rapid initial reaction with TSP followed by a slow transformation of existing Pb-phosphates. Results for granular MAP indicated the presence of Pb phosphates at all distances and incubation times. At the 4 week incubation period, the amount of Pb phosphates was lowest adjacent to the granule and highest at 2300 μm. One possible explanation for this was that another phase was controlling the availability of Pb or P in the vicinity of the granule, thus limiting Pb phosphate formation. At 52 weeks, there was an increase in Pb phosphate minerals present, but the increase occurred at 1600 μm from the granule where pyromorphite was present suggesting that some other phase was limiting P or Pb availability for reaction.

Hettiarachchi et al. (2001) used the same soil contaminated by a Pb/Zn smelter slag and found that PA and a high application of TSP were more effective at reducing bioavailable Pb as measured by the physiologically-based extraction procedure (PBET)

than PR. However, in the other four contaminated materials studied, PR was equally effective as compared to both PA and TSP. This study confirmed the findings of Hettiarachchi et al. (2001) in that PA and TSP were more effective than PR at reducing Pb bioavailability through the formation of insoluble Pb phosphate minerals in the smelter slag contaminated soil. We propose that the smelter slag soil contains more discrete Pb minerals that are dissolved by the acidity created by both PA and TSP, thus allowing more Pb to react with P resulting in more Pb phosphate minerals. Phosphate rock does not produce this acidity; therefore, less Pb phosphates are formed.

It has been suggested that pyromorphite formation is kinetically rapid and aging increases crystallinity in a pure system (Scheckel and Ryan, 2002). However, this study indicated that pyromorphite formation in natural soil environments may actually be rather slow. Hashimoto et al. (2009) also found increased amounts of chloropyromorphite when comparing a P amended, Pb contaminated soil incubated for 380d compared to 7 d. In contaminated soils, there are a number of potential constraints that could delay pyromorphite formation such as P availability, pH, presence of competing cations, accessibility of Pb for reaction, soil organic matter, organic acids, and soil water content, that could lead to the formation of intermediate Pb phosphate phases.

The formation of the Pb phosphate mineral plumbogummite has not been documented in any study using P amendments to stabilize Pb contaminated soils or wastes. However, studies have not attempted to speciate and quantify Pb phosphate formation around individual P granules or droplets. According to Nriagu (1984), the precipitation of plumbogummite during soil formation processes cannot be ignored since the mineral is expected to be more stable than pyromorphite at near neutral pH, provided

that both Pb and phosphate activities are low and Al is available for reaction. Pyromorphite is favored by acidic environments and high P/Pb availabilities. In previous studies, researchers saturated the soil solution with respect to phosphate to induce pyromorphite formation and the systems were homogenized by mixing (Chappell and Scheckel, 2007; Cotter-Howells and Caporn, 1996; Hettiarachchi et al., 2001; Ma et al., 1993, 1995; Scheckel and Ryan, 2002; Scheckel and Ryan, 2004; Yang et al., 2001), which would favor pyromorphite. It was acknowledged that under normal environmental conditions it is inevitable that Pb or P availability could be a rate limiting component for pyromorphite formation (Scheckel and Ryan, 2002), which could lead to the formation of other Pb phosphate minerals. This study was aimed to investigate the Pb speciation changes in the vicinity of an individual P source at the molecular level, which ultimately led to the identification of both plumbogummite and pyromorphite.

For most P sources, the amount of plumbogummite decreased with time with a subsequent increase in pyromorphite (Table 2). This suggests that plumbogummite may be a metastable Pb phosphate mineral that transforms into pyromorphite as P concentrations increase. Plumbogummite is not stable in acid soil environments with elevated Pb and P concentrations (Nriagu, 1984). Therefore, with increasing distance from the point of P application, plumbogummite remains the only Pb phosphate mineral present and this is likely due to low P availability.

Micro-XRD Analysis. Galena was the major mineral species detected by μ-XRD analysis (Table 3). This also was the major mineral species identified using XAS (Table 2). Other minerals that were identified by μ-XRD include cerussite, plumboferrite, magnetoplumbite, plumbogummite, and pyromorphite. Figure 4A is an example μ-XRD

pattern for PA incubated for 52 weeks that indicates the presence of chloropyromorphite and plumboferrite 400 μm from the point of application while [Figure 4](#)B is an example for PA also at 52 weeks indicating the presence of plumbogummite 1500 μm. Most interestingly, XRD was able to confirm many of the same trends that were discovered using XAS. For example, at the 4 week incubation, identification of plumbogummite and pyromorphite (Pb phosphates) by XRD was limited primarily to the area adjacent to the point of application, which was similar to the results using XAS. However, XAS on many occasions identified Pb phosphates at much greater distances than XRD, but XAS can determine mineral speciation on both amorphous and crystalline materials at a much lower detection limit, while XRD was limited to only crystalline species. Crystallinity of Pb phosphates may be an issue at early incubation times At the 52 week incubation, Pb phosphate minerals can be identified by XRD at greater distances from the point of application indicating an increase in crystallinity. Pyromorphites have increased crystallinity, more distinguishable morphology, and greater stability with time after formation (Scheckel and Ryan, 2002; Stack et al., 2004), which would facilitate identification by XRD.

We have proposed that plumbogummite or plumbogummite-like minerals could be metastable Pb phases during the formation of pyromorphite. In addition, species could be poorly crystalline or amorphous in nature and would not strongly defract X-rays making them more difficult to detect by XRD. However, μ-XRD is a quick and powerful tool when coupled with μ-XAS. The use of μ-XRD supported the findings of the XAS work and reduced the inherent uncertainty in the linear combination fitting procedure.

Environmental Implications. All P amendments were able to induce Pb phosphate

formation *in situ*, thus potentially reducing Pb bioavailability. Pyromorphite formation is preceded by the formation of other metastable Pb phosphate minerals, such as plumbogummite, which was not been previously reported. This further suggests that Pb bioavailability may change with time. Fluid P amendments are superior at inducing Pb phosphate formation over a much greater area than granular P sources, suggesting greater P diffusion and subsequent availability of P for reaction with Pb. The outward rate of P movement may have been slower in the granules due to their hygroscopic nature and the influx of water upon placement into the moist soil (Hettiarachchi et al., 2006). In general, PA was the most effective P amendment at producing Pb phosphates. This can be attributed to high levels of available P and the acidity of PA that can make Pb more readily available for reaction through the dissolution of discrete Pb minerals (Cao et al., 2003). Triple super phosphate was the most effective granular source at forming Pb phosphates. As a result, PA and TSP were the most effective P amendments at inducing Pb phosphate formation in this material, but monitoring is necessary to assure stability of Pb phosphates over time and to limit the impact of P on the environment.

References

Adriano, D.C. 2001. Trace elements in terrestrial environments: Biogeochemistry, bioavailability, and risks of metals. 2nd ed. Springer-Verlag, New York, NY

Agency for Toxic Substances and Disease Registry. 2005. ToxFAQS for lead [Online]. Available at www.atsdr.cdc.gov/tfacts13.html (accessed 10 Oct. 2006). ATSDR, Atlanta, GA.

Baker, L.R., G.M. Pierzynski, G.M. Hettiarachchi, K.G. Scheckel, and M. Newville. 2012. Zinc speciation in proximity to phosphate application points in a Pb/Zn smelter contaminated soil. J. Environ. Qual. 41:1865-1873

Basta, N.T., J.A. Ryan, and R.F. Chaney. 2005. Trace element chemistry in residual-treated soil: Key concepts and metal bioavailability. J. Environ. Qual. 34:49-63.

Bremner, J.M., and C.S. Mulvaney. 1982. Salicylic acid thiosulfate modification of the Kjeldhal method to include nitrate and nitrite. p. 621. *In* R.H. Miller and D.R. Keeney (ed.) Methods of soil analysis. Part 2. Am. Soc. Agron., Madison, WI.

Brown, M. J. and S. Margolis. 2012. Lead in drinking water and human blood lead levels in the United States. Center for Disease Control and Prevention. MMWR Supplement. Vol. 61 [Online]. Available at http://www.cdc.gov/mmwr/pdf/other/su6104.pdf (accessed 28 Sep. 2012). CDC, Atlanta, GA.

Butkus, M. A., & Johnson, M. C. (2011). Reevaluation of phosphate as a means of retarding lead transport from sandy firing ranges. Soil and Sediment Contamination, 20(2), 172-187. Retrieved from www.scopus.com

Cao, X., L.Q. Ma, M. Chen, S.P. Singh, and W.G. Harris. 2002. Impacts of phosphate amendments on lead biogeochemistry at a contaminated site. Environ. Sci. Technol. 36:5296-5304.

Cao, R.X., L.Q. Ma, M. Chen, S.P. Singh, and W.G. Harris. 2003. Phosphate-induced metal immobilization in a contaminated site. Environ. Pollut. 122:19-28.

Chappell, M.A., and K.G. Scheckel. 2007. Pyromorphite formation and stability after quick lime neutralization in the presence of soil and clay sorbents. Environ. Chem. 4:109-113.

Chen, S.B., Y.G. Zhu, and Y.B. Ma. 2006. The effect of grain size of rock phosphate amendment on metal immobization in contaminated soils. J. Hazard Mater. 134:74-79.

Cotter-Howells, J., and S. Caporn. Remediation of contaminated land by formation of heavy metal phosphates. Appl. Geochem. 11:335-342.

Debela, F., Arocena, J. M., Thring, R. W., & Whitcombe, T. (2010). Organic acid-induced release of lead from pyromorphite and its relevance to reclamation of pb-contaminated soils. Chemosphere, 80(4), 450-456. Retrieved from www.scopus.com

Gee, G.W., and J.W. Bauder. 1986. Particle size analysis. p. 399-404. *In* A. Klute (ed.) Methods of soil analysis. Part 1. 2nd ed. Agron. Monogr. 9. ASA and SSSA, Madison, WI.

Hammersley, A.P., S.O. Svensson, M. Hanfland, A.N. Fitch, and D. Häusermann. 1996. Two-dimensional detector software: From real detector to idealized image or two-theta scan. High Press. Res. 14:235-248.

Hashimoto, Y., Takaoka, M., Oshita, K., & Tanida, H. (2009). Incomplete transformations of pb to pyromorphite by phosphate-induced immobilization investigated by X-ray absorption fine structure (XAFS) spectroscopy. Chemosphere, 76(5), 616-622. Retrieved from www.scopus.com

Hettiarachchi, G.M., E. Lombi, M.J. McLaughlin, D. Chittleborough, and P. Self. 2006. Density changes around phosphorus granules and fluid bands in a calcareous soil. Soil Sci. Soc. Am. J. 70:960-966.

Hettiarachchi, G.M., and G.M. Pierzynski. 2004. Soil lead bioavailability and in situ remediation of lead-contaminated soils: A review. Environ. Prog. 23:78-93.

Hettiarachchi, G.M., G.M. Pierzynski, and M.D. Ransom. 2000. In situ stabilization of soil lead using phosphorus and manganese oxide. Environ. Sci. Tech. 34:4614-4619.

Hettiarachchi, G.M., G.M. Pierzynski, and M.D. Ransom. 2001. In situ stabilization of lead using phosphorus. J. Environ. Qual. 30:1214-1221.

Isaure, M.-P., A. Laboudigue, A. Manceau, G. Sarret, C. Tiffreau, P. Trocellier, G. Lamble, J.-L. Hazemann, and D. Chateigner. 2002. Quantitative Zn speciation in

a contaminated dredged sediment by μ-PIXE, μ-SXRF, EXAFS spectroscopy and principal components analysis. Geochim. Cosmochim. Acta 66:1549-1567.

Jackson, M.L. 1975. Soil chemical analysis-advanced course. 2nd ed. Dep. Soil Sci., Univ. of Wisconsin, Madison, WI.

Jackson, M.L., C.H. Lim, and L.W. Zelazny. 1986. Oxides, hydroxides and aluminosilicates. p. 101-150. *In* A. Klute (ed.) Methods of soil analysis. Part 1. 2nd ed. Agron. Monogr. 9. ASA and SSSA, Madison, WI.

Jaynes, W.F., and J.M. Bigham. 1986. Multiple cation-exchange capacity measurements on standard clays using a commercial mechanical extractor. Clays Clay Miner. 34:93-98.

JCPDS-International Centre for Diffraction Data. 1987. Powder diffraction file inorganic phases search manual (Hanawalt method). JCPDS, Swarthmore, PA.

Lin, C.W., J. Lian, and H.H. Fang. 2005. Soil lead immobilization using phosphate rock. Water Air Soil Pollut. 161:113-123.

Lindsay, W.L. 1979. Chemical equilibria in soils. Wiley, New York, NY.

Kilgour, D.W., R.B. Moseley, M.O. Barnett, K.S. Savage, and P.M. Jardine. Potential negative consequences of adding phosphorus-based fertilizers to immobilize lead in soil. J. Environ. Qual. 37:1736-1740.

Lombi, E., M.J. McLaughlin, C. Johnston, R.D. Armstrong, and R.E. Holloway. 2005. Mobility, solubility, and lability of fluid and granular forms of P fertilizer in calcareous and non-calcareous soils under laboratory conditions. Plant Soil 269:25-34.

Ma, Q.Y., T.J. Logan, and S.J. Traina. 1995. Lead immobilization from aqueous solutions and contaminated soils using phosphate rocks. Environ. Sci. Technol. 29:1118-1126.

Ma, Q.Y., T.J. Logan, S.J. Traina, and J.A. Ryan. 1994. Effects of NO_3^-, Cl^-, F^-, SO_4^{2-}, and CO_3^{2-} on Pb^{2+} immobilization by hydroxyapatite. Environ. Sci. Technol. 28:408-418.

Ma, Q.Y., S.J. Traina, T.J. Logan, and J.A. Ryan. 1993. In situ lead immobilization by apatite. Environ. Sci. Technol. 27:1803-1810.

Manceau, A., M.A. Marcus, and N. Tamura. 2002a. Quantitative speciation of heavy

metals in soils and sediments by X-ray techniques. Rev. Mineral. Geochem. 49:321-428.

Manceau, A., N. Tamura, M.A. Marcus, A.A. MacDowell, R.S. Celestre, R.E. Sublett, G. Sposito, and H.A. Padmore. 2002b. Deciphering Ni sequestration in soil ferromanganese nodules by combining X-ray fluorescence, absorption, and diffraction at micrometer scales of resolution. Am. Mineral. 87:1494-1499.

Mehlich, A. 1984. Mehlich 3 soil test extractant: A modification of Mehlich-2 extractant. Commun. Soil Sci. Plant Anal. 15(12): 1409-1416.

Mench, M., V. Didier, M. Loffler, Am. Gomez, and P. Masson. 1994. A mimicked in-situ remediation study of metal-contaminated soils with emphasis on Cd and Pb. J. Environ. Qual. 23:58-63.

McGowen, S.L., N.T. Basta, and G.O. Brown. 2001. Use of diammonium phosphate to reduce heavy metal solubility and transport in smelter-contaminated soil. J. Environ. Qual. 30:493-500.

Nriagu, J.O. 1974. Lead orthophosphates-IV. Formation and stability in the environment. Geochim. Cosmochim. Acta 38:887-989.

Nriagu, J.O. 1984. Formation and stability of base metal phosphates in soils and sediments. p. 318-329. *In* J.O. Nriagu and P.B. Moore (ed.) Phosphate Minerals. Springer, London.

Ostergren, J.D., G.E. Brown Jr., G.A. Parks, and T.N. Tingle. 1999. Quantitative speciation of lead in selected mine tailings from Leadville, CO.

Porter, S.K, K.G. Scheckel, C.A. Impellitteri, and J.A. Ryan. 2004. Toxic metals in the environment: thermodynamic considerations for possible immobilization strategies for Pb, Cd, As, and Hg. Crit. Rev. Environ. Sci. Technol. 34: 495-604.

Ravel, B., and M. Newville. 2005. ATHENA, ARTEMIS, HEPHAESTUS: Data analysis for X-ray absorption spectroscopy using IFEFFIT. J. Synchrotron Radiat. 12:537-541.

Roberts, D.R., A.C. Scheinost, D.L. Sparks. 2002. Zinc speciation in a smelter-contaminated soil profile using bulk and microspectroscopic techniques. Envron. Sci. Technol. 36:1742-1750.

Ruby, M.V., A. Davis, and A. Ncholson. 1994. In situ formation of lead phosphates in

soils as a method to immobilize lead. Environ. Sci. Technol. 28:646-654.

Ryan, J.A.,   K.G Scheckel, W.R Berti, S.L Brown, S.W Casteel, R.L Chaney, J. Hallfrisch, M. Doolan, P. Grevatt, M. Maddaloni, and D. Mosby. 2004. Peer reviewed: reducing children's risk from lead in soil. Environ. Sci. Technol. 38: 18A-24A.

Scheckel, K.G., and J.A. Ryan. 2002. Effects of aging and pH on dissolution kinetics and stability of chloropyromorphite. Environ. Sci. Technol. 36:2198-2204.

Scheckel, K.G., and J.A. Ryan. 2004. Spectroscopic speciation of lead in phosphate-amended soils. J. Environ. Qual. 33:1288-1295.

Scheckel, K.G., R.L. Chaney, N.T. Basta, and J.A. Ryan. 2009. Advances in assessing bioavailability of metal (loid) s in contaminated soils. Adv. Agron. 104:1-52.

Sims, J.T., and G.M. Pierzynski. 2005. Chemistry of phosphorus in soils. *In* M.A. Tabatabai and D.L. Sparks (ed.) Chemical processes in soils. SSSA Book Ser. 8. SSSA. Madison, WI.

Sposito, G., L.J. Lund, and A.C. Chang. 1982. Trace metal chemistry in arid-zone field soils amended with sewage sludge: I. Fractionation of Ni, Cu, Zn, Cd, and Pb in solid phases. Soil Sci. Soc. Am. J. 46:260-264.

Stack, A.G., R. Erni, N.D. Browning, and W.H. Casey. 2004. Pyromorphite growth on lead-sulfide surfaces. Environ. Sci. Technol. 38:5529-5534.

Yang, J., D.E. Mosby, S.W. Casteel, and R.W. Blanchar. 2001. Lead immobilization using phosphoric acid in a smelter-contaminated urban soil. Environ. Sci. Technol. 35:3553-3559.

Yoon, J.K., X.D. Cao, and L.Q. Ma. 2007. Application methods affect phosphorus-induced lead immobilization from a contaminated soil. J. Environ. Qual. 36:373-378.
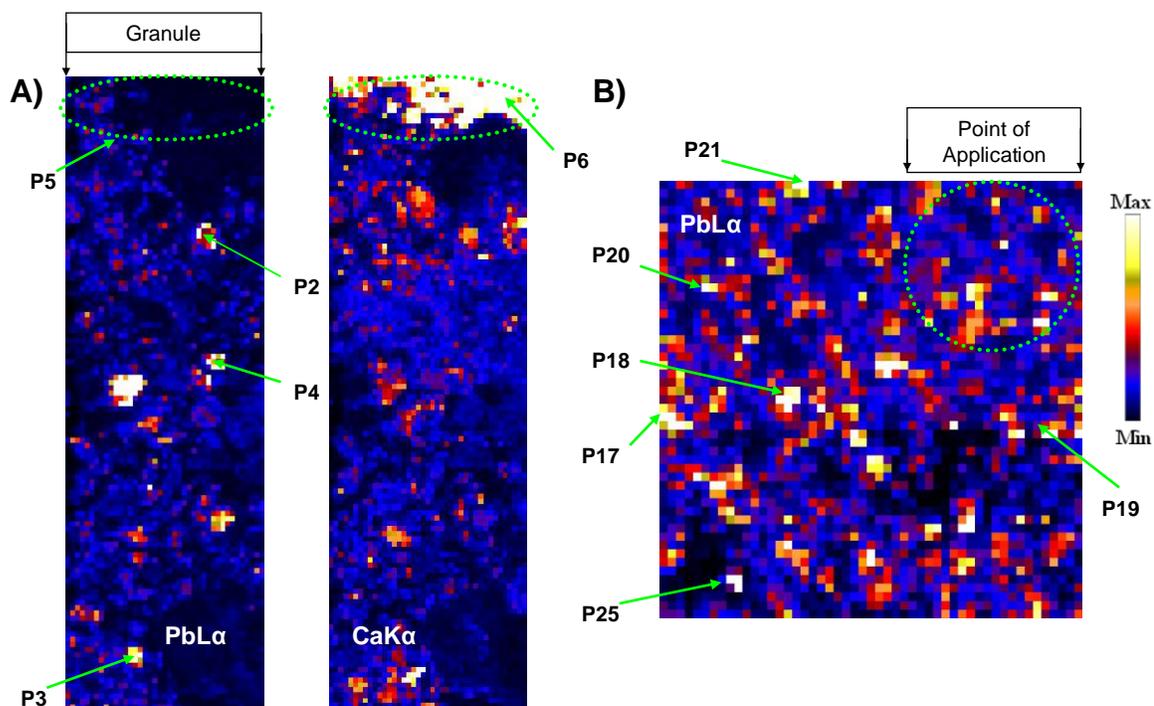
Figure 1. Micro-X-ray fluorescence maps of a) Pb and Ca for soil incubated with PR for 1 month and b) Pb for soil incubated with PA for 1 month. Area of a single map is a) 2000- by 6000-μm and b) 2500- by 2500- μm. The color scheme used ranges from white or yellow for high fluorescence signal to blue or black for low fluorescence signal. Shading is relative across each map. The markers P1 to P6 in a) and P17 to P25 in b) represent locations for which μ-X-ray absorption near-edge structure (XANES) and μ-X-ray diffraction (XRD) analyses were conducted. Calcium is shown in a) to illustrate the location of a PR granule.
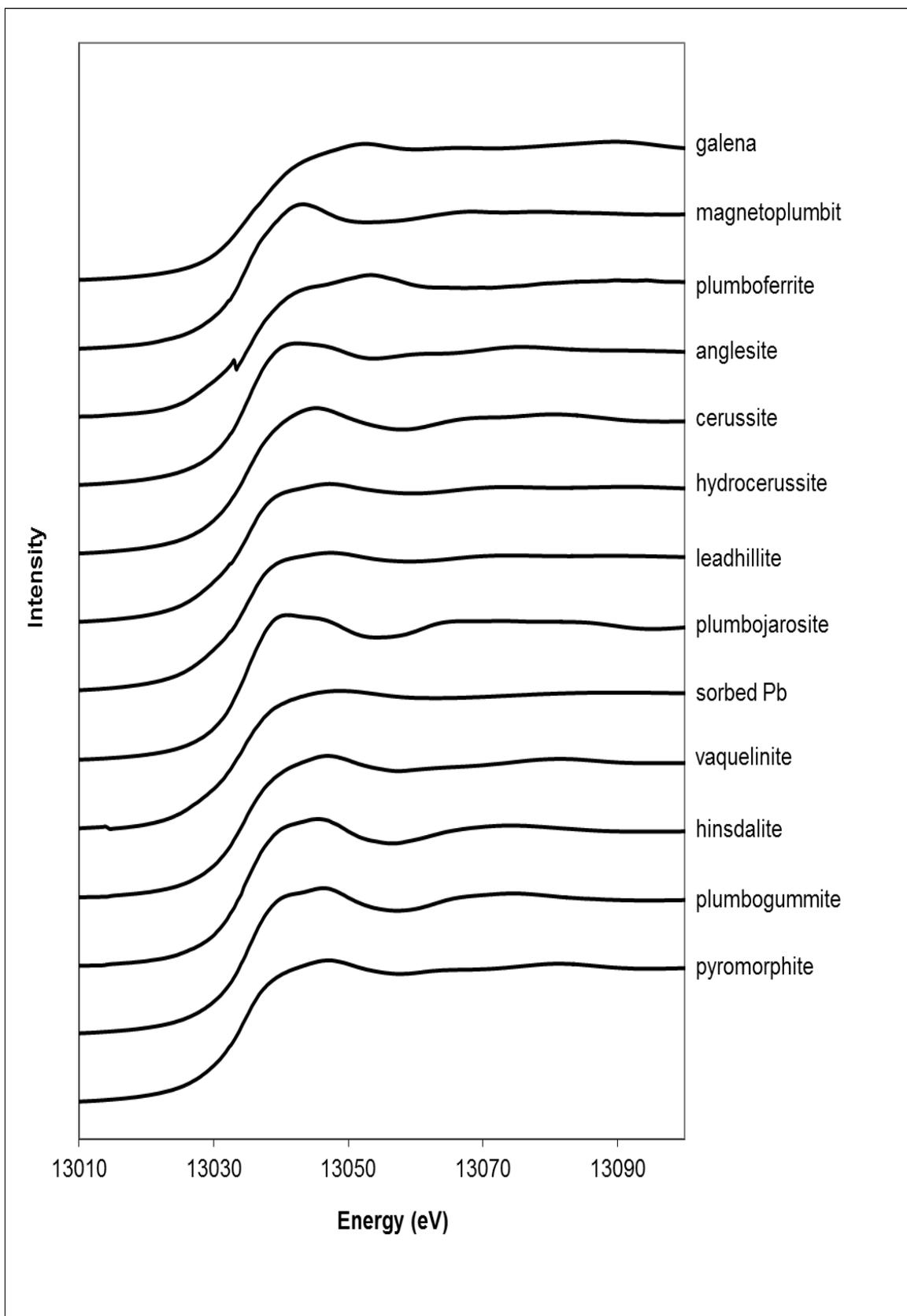
Figure 2. A) Normalized Pb μ-XANES spectra for all standard Pb compounds used for linear combination fitting
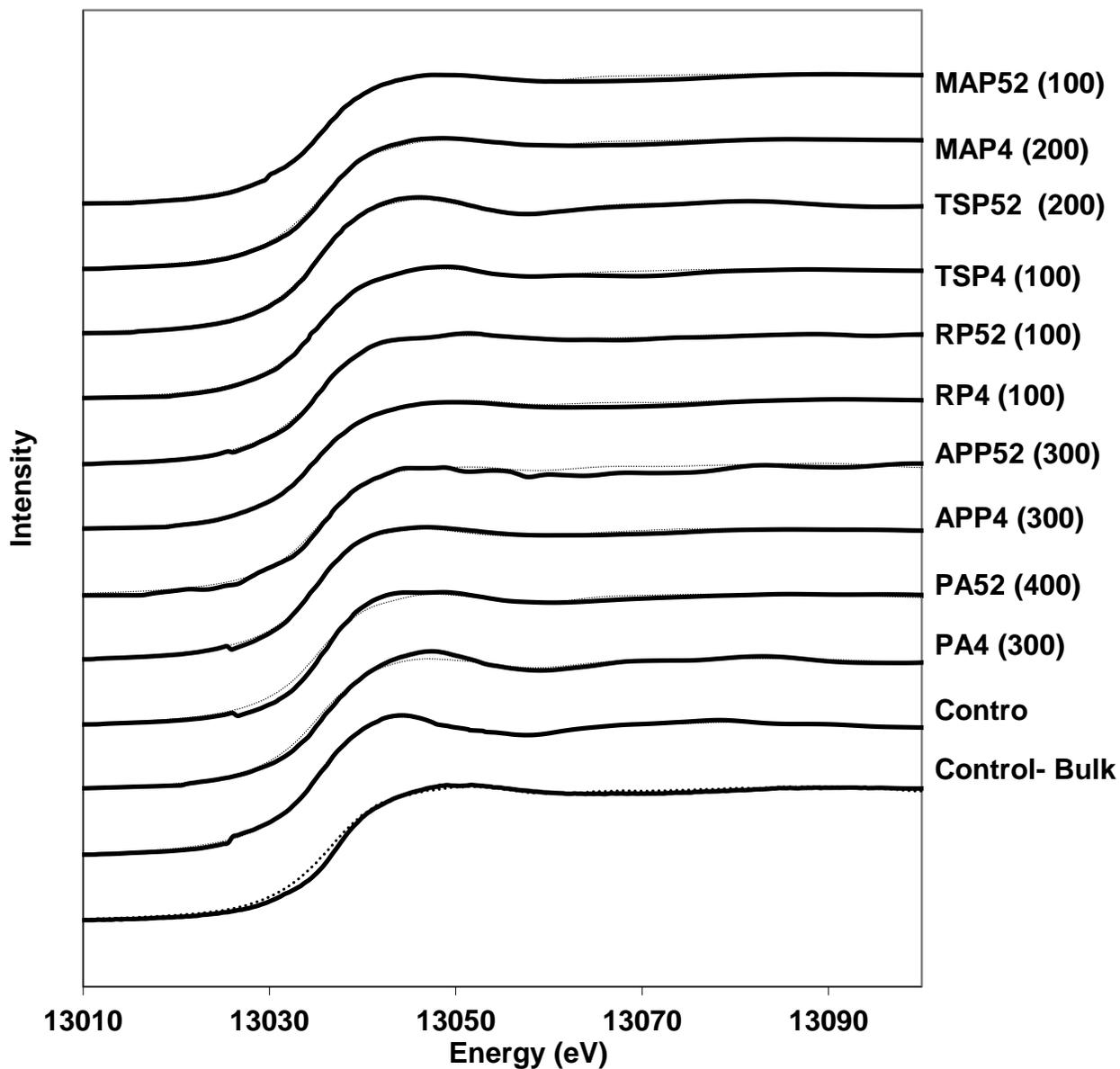
Figure 2. B) Normalized Pb μ-XANES spectra (solid lines) for the Pb L-edge X-ray absorption spectroscopic data. Data were collected from points 100- to 400-μm from the edge of a granule or the center of a droplet, except the control which is a representative spectra from the incubated treatment with no P amendment, and the spectra for bulk samples of the control. Dotted lines indicate the best linear combination fits using all the standard Pb mineral compounds. Control-bulk: bulk-XANES-unamended control, Control: representative μ-XANES spectra-unamended sample, PR: phosphate rock, TSP: triple super phosphate, PA: phosphoric acid, APP: ammonium polyphosphate. The numbers 4 and 52 indicate the incubation period in weeks.
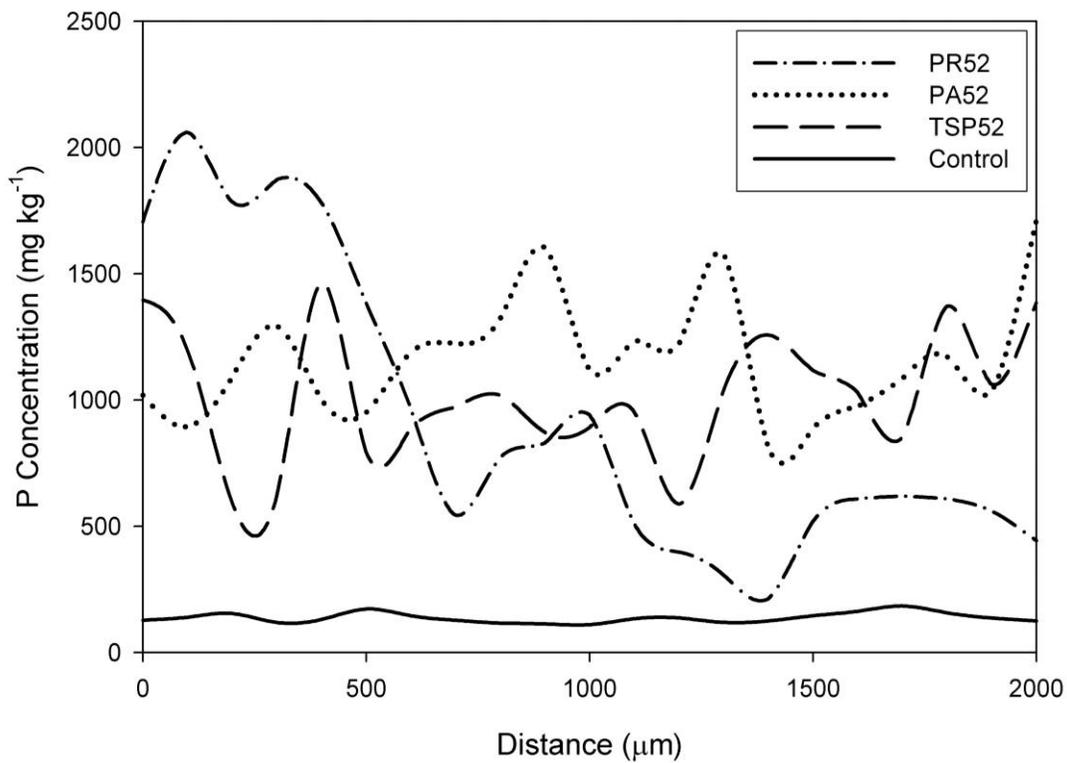
Figure 3. A radial distribution plot at 52 weeks for P generated by using μ-XRF maps for soils treated with PR, PA, and TSP. Point of application is at 0 μm. The solid line represents the background P concentration measured across the control soil. PR52: phosphate rock at 52 weeks, PA52: phosphoric acid at 52 weeks, TSP52: triple super phosphate at 52 weeks, and control: amended sample.

Figure 4A
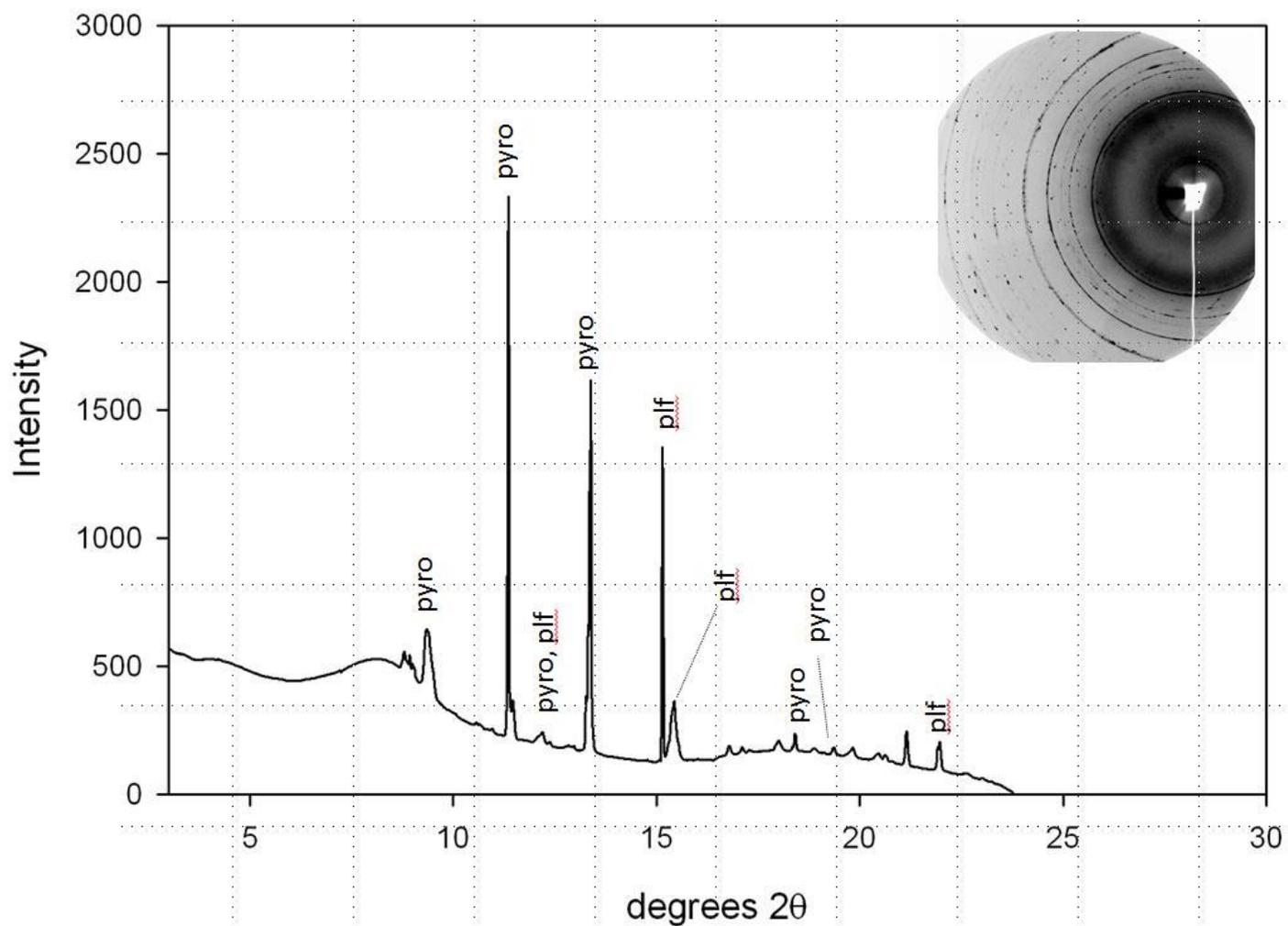
Figure 4. A) Micro-XRD pattern for treatment PA52 at 400 μm from the center of treatment. Original Debye-Sherer rings are located in the top-right hand corner of the graph. Species detected are pyro (chloropyromorphite [$Pb_5(PO_4)_3(Cl)$]) with d-spacings of 2.97, 2.89, 4.13, 3.27, 2.06, and 1.92) and plf (plumboferrite [$Pb_2Mn_{0.2}Mg_{0.1}Fe_{10.6}O_{18.4}$] with d-spacings of 2.64, 2.97, 2.44, and 1.68).

Figure 4B
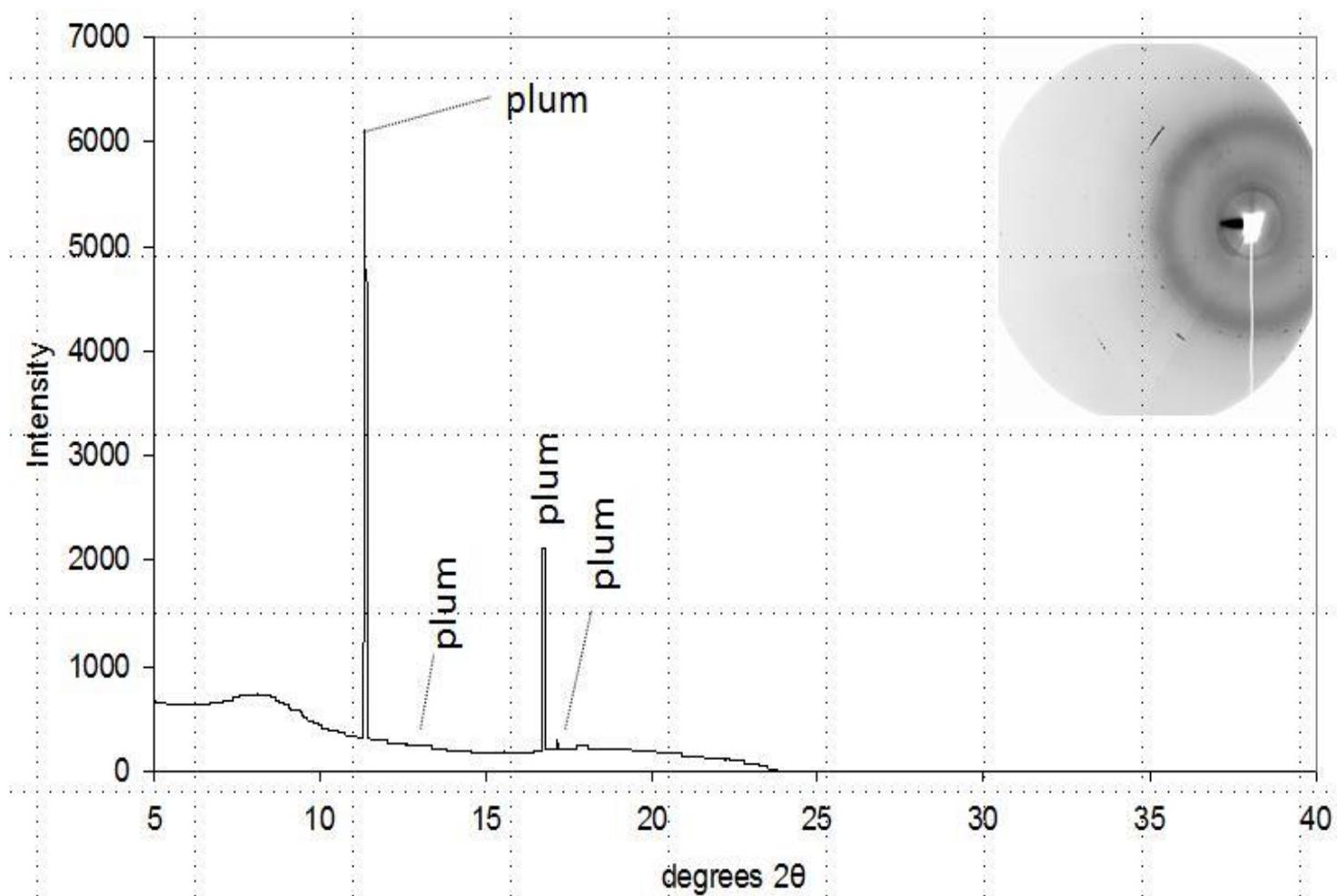
Figure 4. B) Micro-XRD pattern for PA52 at 1500 μm from the center of the treatment. All peaks are assigned to plumbogummite with d-spacings of 2.97, 5.70, 3.50, 2.22, 2.21, 1.90, 3.44, and 5.57.

Table 1. Selected soil properties.

Property	Value
pH	6.4
Total organic C, g kg^{-1}	39.7
Total P, mg kg^{-1}	152
Mehlich-3 extractable P, mg kg^{-1}	18.0
Na-CBD Fe mg kg^{-1}	38000
Total Pb, mg kg^{-1}	24300
Total Zn, mg kg^{-1}	72900
Total Cd, mg kg^{-1}	103
Cation exchange capacity, cmolc kg^{-1}	42.3
Sand, mg kg^{-1}	764
Silt, mg kg^{-1}	164
Clay, mg kg^{-1}	72

Table 2. Percentages of Pb species from selected POIs for control and P treated soils as determined by linear combination fitting of μ-X-ray absorbtion near-edge structure (μ-XANES) spectra 4 and 52 weeks after P amendment addition. Typical uncertainties in the percentages listed for each standard component are 5%.

Sample †	Distance ‡	Ce#	Ga	Pg	Py	Mp	Pf	Ag	SPb	χ2††
Control	--	54	3	--	--	43	--	--	--	0.18
Control	--	--	14	--	--	--	4	18	64	0.62
Control	--	--	51	--	--	--	9	40		0.58
PR4	100	--	36	55	--	6	3	--	--	0.72
PR4	2200	62	30	115	--	--	--	--	--	0.22
PR4	5100	--	55	1	--	16	--	--	28	0.28
PR52	100	--	22	26	19	--	33	--	--	0.19
PR52	900	36	14	50	--	--	--	--	--	0.15
PR52	1200	--	44	5	--	--	23	29	--	0.23
TSP4	100	--	43	35	8	--	13	--	--	0.30
TSP4	1800	--	59	31	--	10	--	--	--	0.55
TSP4	5200	--	47	31	--	17	6	--	--	0.17
TSP52	200	67	--	14	19	--	--	--	--	0.66
TSP52	2000	--	45	33	--	--	--	22	--	0.27
TSP52	3100	40	24	36	--	--	--	--	--	0.19
MAP4	200	--	48	17	--	36	--	--	--	0.24
MAP4	1500	--	--	8	--	--	28	25	39	0.86
MAP4	2300	--	60	32	--	--	9	--	--	0.39
MAP52	100	--	51	31	--	18	--	--	--	0.10
MAP52	1600	31	--	43	15	11	--	--	--	0.86
MAP52	3600	--	63	30	--	--	--	--	7	0.28
PA4	300	--	49	32	--	--	19	--	--	0.28
PA4	1800	--	73	27	--	--	--	--	--	0.11
PA4	2500	36	47	17	--	--	--	--	--	0.83
PA52	400	--	18	--	39	9	35	--	--	0.81
PA52	1500	--	43	57	--	--	--	--	--	0.10
PA52	3300	--	52	48	--	--	--	--	--	0.13
APP4	300	30	11	38	22	--	--	--	--	0.50
APP4	2400	--	37	56	7	--	--	--	--	0.37
APP4	3600	--	89	11	--	--	--	--	--	0.38
APP52	300	--	21	--	56	5	19	--	--	0.56
APP52	1700	--	45	10	--	37	--	--	8	0.17
APP52	4200	--	65	14	--	21	--	--	--	0.11

† Control: non-P amended; PR: Phophate rock; TSP: Triple super phosphate; MAP: Monammonium phosphate; PA: Phosphoric acid; APP: Ammonium polyphosphate. Number following treatment indicates incubation time (4 or 52 weeks).

‡ Distance in μm from the P treatment. For fluid sources (PA and APP) this distance begins at the approximate center of the point of application. For granular sources (PR, TSP, and MAP) this distance begins at the edge of the granule. Points of interest for the controls were taken randomly where high relative Pb concentrations were present.

Ce: Cerussite, Ga: Galena, Pg: Plumbogummite, Py: Pyromorphite, Mp: Magnetoplumbite, Pf: Plumboferrite, Ag: Anglesite, SPb: Sorbed Pb

†† Values closer to 0 and ≤ 1 indicate more reliable fits.

Table 3. A summary of μ-XRD analysis for Pb POI's that corresponds to Pb POI's selected for μ-XAS in Table 2.

Sample†	Distance ‡	Minerals Detected by μ-XRD Analysis
Control	-	Galena, Cerussite
Control	-	Galena, Cerussite
PR4	100	Galena, Plumbogummite
PR4	2200	Cerussite
PR4	5100	Galena
PR52	100	Pyromorphite, Plumboferrite
PR52	900	Cerussite, Plumbogummite
PR52	1200	Galena, Plumboferrite
TSP4	100	Galena, Plumbogummite
TSP4	1800	Galena
TSP4	5200	Galena
TSP52	200	Cerussite, Pyromorphite
TSP52	2000	Galena
TSP52	3100	Cerussite, Plumbogummite
MAP4	200	Galena, Magnetoplumbite
MAP4	1500	Plumboferrite
MAP4	2300	Galena
MAP52	100	Galena
MAP52	1600	Plumbogummite
MAP52	3600	Galena
PA4	300	Galena
PA4	1800	Galena
PA4	2500	Cerussite, Galena
PA52	400	Pyromorphite, Plumboferrite
PA52	1500	Plumbogummite
PA52	3300	Galena, Plumbogummite
APP4	300	Plumbogummite, Pyromorphite
APP4	2400	Galena, Plumbogummite
APP4	3600	Galena
APP52	100	Pyromorphite

† Control: non-P amended; PR: Phophate rock; TSP: Triple super phosphate; MAP: Monammonium phosphate; PA: Phosphoric acid; APP: Ammonium polyphosphate. Number following treatment indicates incubation time (4 or 52 weeks).

‡ Distance in μm from the P treatment. For fluid sources (PA and APP) this distance begins at the approximate center of the point of application. For granular sources (PR, TSP, and MAP) this distance begins at the edge of the granule. Points of interest for the controls were taken randomly where high relative Pb concentrations were present.

Table 4. A summary of Pb speciation results with different x-ray techniques

Sample	Laboratory based-XRD	Micro-XRD	Bulk-XANES	Micro- XANES
Control	None identified	cerussite, galena	cerussite, galena, plumboferrite	cerussite, galena, sorbed Pb, magnetoplumbite, plumboferrite, anglesite
PR4	_	galena, cerussite, plumbogummite	_	cerussite, galena, plumbogummite, magnetoplumbite, plumboferrite, sorbed Pb
PR52	_	pyromorphite, plumboferrite, cerussite, plumbogummite, galena	_	plumbogummite, plumboferrite, galena, cerussite pyromorphite, anglesite
TSP4	_	galena, plumbogummite,	_	galena, plumbogummite, plumboferrite, pyromorphite, magnetoplumbite
TSP52	_	cerussite, pyromorphite, plumbogummite, galena	_	cerussite, galena, plumbogummite, pyromorphite, anglesite
MAP4	_	galena, magnetoplumbite, plumboferrite, plumbogummite,	_	galena, plumbogummite, pyromorphite, plumboferrite, anglesite, sorbed Pb
MAP52	_	Plumbogummite, galena	_	galena, plumbogummite, magnetoplumbite, cerussite, pyromorphite
PA4	_	galena, cerussite	_	galena, plumbogummite, plumboferrite, cerussite

PA52	_	pyromorphite, plumboferrite, galena, plumbogummite,	_	Galena, plumbogummite, pyromorphite, plumboferrite, magnetoplumbite
APP4	_	plumbogummite, pyromorphite, galena	_	plumbogummite, galena, pyromorphote, cerussite
APP52	_	pyromorphite, galena, magnetoplumbite	_	Galena, pyromorphite, plumbogummite, plumboferrite, magnetoplumbite